JCI The Journal of Clinical Investigation

Uterine-specific p53 deficiency confers premature uterine senescence and promotes preterm birth in mice

Yasushi Hirota, … , Heather B. Bradshaw, Sudhansu K. Dey

J Clin Invest. 2010;120(3):803-815. https://doi.org/10.1172/JCI40051.

Research Article **Reproductive biology**

Many signaling pathways that contribute to tumorigenesis are also functional in pregnancy, although they are dysregulated in the former and tightly regulated in the latter. Transformation-related protein 53 (*Trp53*), which encodes p53, is a tumor suppressor gene whose mutation is strongly associated with cancer. However, its role in normal physiological processes, including female reproduction, is poorly understood. Mice that have a constitutive deletion of *Trp53* exhibit widespread development of carcinogenesis at early reproductive ages, compromised spermatogenesis, and fetal exencephaly, rendering them less amenable to studying the role of p53 in reproduction. To overcome this obstacle, we generated mice that harbor a conditional deletion of uterine *Trp53* and examined pregnancy outcome in females with this genotype. These mice had normal ovulation, fertilization, and implantation; however, postimplantation uterine decidual cells showed terminal differentiation and senescence-associated growth restriction with increased levels of phosphorylated Akt and p21, factors that are both known to participate in these processes in other systems. Strikingly, uterine deletion of *Trp53* increased the incidence of preterm birth, a condition that was corrected by oral administration of the selective COX2 inhibitor celecoxib. We further generated evidence to suggest that deletion of uterine *Trp53* induces preterm birth through a COX2/PGF synthase/$PGF_{2\alpha}$ pathway. Taken together, our observations underscore what we believe to be a new critical role of uterine p53 in parturition.

Uterine-specific p53 deficiency confers premature uterine senescence and promotes preterm birth in mice

Yasushi Hirota,[1] Takiko Daikoku,[1] Susanne Tranguch,[1] Huirong Xie,[1] Heather B. Bradshaw,[2] and Sudhansu K. Dey[1]

[1]Division of Reproductive Sciences, The Perinatal Institute, Cincinnati Children's Hospital Medical Center, University of Cincinnati College of Medicine, Ohio. [2]Department of Psychological and Brain Sciences, Kinsey Institute for Research in Sex, Gender and Reproduction, Indiana University, Bloomington.

Many signaling pathways that contribute to tumorigenesis are also functional in pregnancy, although they are dysregulated in the former and tightly regulated in the latter. Transformation-related protein 53 (*Trp53*), which encodes p53, is a tumor suppressor gene whose mutation is strongly associated with cancer. However, its role in normal physiological processes, including female reproduction, is poorly understood. Mice that have a constitutive deletion of *Trp53* exhibit widespread development of carcinogenesis at early reproductive ages, compromised spermatogenesis, and fetal exencephaly, rendering them less amenable to studying the role of p53 in reproduction. To overcome this obstacle, we generated mice that harbor a conditional deletion of uterine *Trp53* and examined pregnancy outcome in females with this genotype. These mice had normal ovulation, fertilization, and implantation; however, postimplantation uterine decidual cells showed terminal differentiation and senescence-associated growth restriction with increased levels of phosphorylated Akt and p21, factors that are both known to participate in these processes in other systems. Strikingly, uterine deletion of *Trp53* increased the incidence of preterm birth, a condition that was corrected by oral administration of the selective COX2 inhibitor celecoxib. We further generated evidence to suggest that deletion of uterine *Trp53* induces preterm birth through a COX2/PGF synthase/$PGF_{2\alpha}$ pathway. Taken together, our observations underscore what we believe to be a new critical role of uterine p53 in parturition.

Introduction

Pregnancy is a complex process. Ovulation, fertilization, preimplantation embryo development, oviductal embryo transport, embryo implantation, uterine decidualization, placentation, and parturition are all critical, and failure at any of these stages compromises pregnancy outcome. Implantation is the first encounter between embryo and mother, while parturition is the end of this encounter, although soluble factors from the uterus and/or embryo influence the embryo-uterine dialogue prior to implantation. Therefore, implantation and parturition are — conceptually, physiologically, and clinically — distinct conundrums with different molecular and genetic signatures. Although implantation failure is a significant cause of infertility and a clinical issue in in vitro fertilization programs, preterm birth and prematurity are problems with consequences that continue beyond birth, posing huge long-term social and economic liabilities.

Premature delivery accounts for 75% of early neonatal morbidity and mortality, making this disorder a global clinical, social, and economic burden (1). About 13 million premature births and more than 3 million stillbirths occur each year. Prematurity is a direct cause of nearly 30% of all neonatal deaths, totaling more than 1 million each year. In addition, many babies that survive premature birth suffer serious long-term disabilities (2). According to the 2006 report of the Institute of Medicine, National Academies of Sciences, the total cost of preterm birth is estimated to be at least $26 billion a year in the United States (3). Therefore, there is an urgent need to research new approaches for combating this public health concern.

In the present study, we used a mouse model of conditional deletion of uterine *Trp53* to demonstrate that p53 deficiency conferred premature uterine senescence and promoted preterm birth.

Several signaling pathways that function during pregnancy are also active during tumorigenesis, the difference being their tight regulation during pregnancy but dysregulation during tumorigenesis (4). Mutation of *Trp53* is found in a variety of cancers (5); however, its roles in normal physiological processes, including female reproduction, remain poorly understood. A recent study reported that mice constitutively deleted of *Trp53* ($Trp53^{-/-}$ mice) have implantation failure caused by downregulation of uterine leukemia inhibitory factor (LIF) on day 4 of pregnancy (with day 1 defined as the day the vaginal plug forms) (6). These systemic null mice, however, begin to die of cancer as early as 2 months of age (7), and a number of $Trp53^{-/-}$ fetuses, especially females, die prematurely due to the development of exencephaly (8). In addition, $Trp53^{-/-}$ males have compromised spermatogenesis (9). Such complications make these mice less than appropriate for studying female reproductive phenotypes devoid of other systemic and male effects. Therefore, we generated mice with conditional deletion of uterine *Trp53* by crossing floxed *Trp53* mice ($Trp53^{loxP/loxP}$ mice; ref. 10) with progesterone (P_4) receptor–Cre (*PR*-Cre) transgenic mice ($Pgr^{Cre/+}$ mice; ref. 11) and examined critical events during the course of pregnancy. Although all females with uterine deletion of *Trp53* showed normal implantation, more than 50% had preterm birth with neonatal death associated with premature uterine senescence. Further studies to unravel the underlying mechanism revealed that p21 and phosphorylated Akt (pAkt) contributed to premature uterine senescence and that activation of the Akt/COX2 signaling

Conflict of interest: The authors have declared that no conflict of interest exists.
Citation for this article: *J Clin Invest.* 2010;120(3):803–815. doi:10.1172/JCI40051.

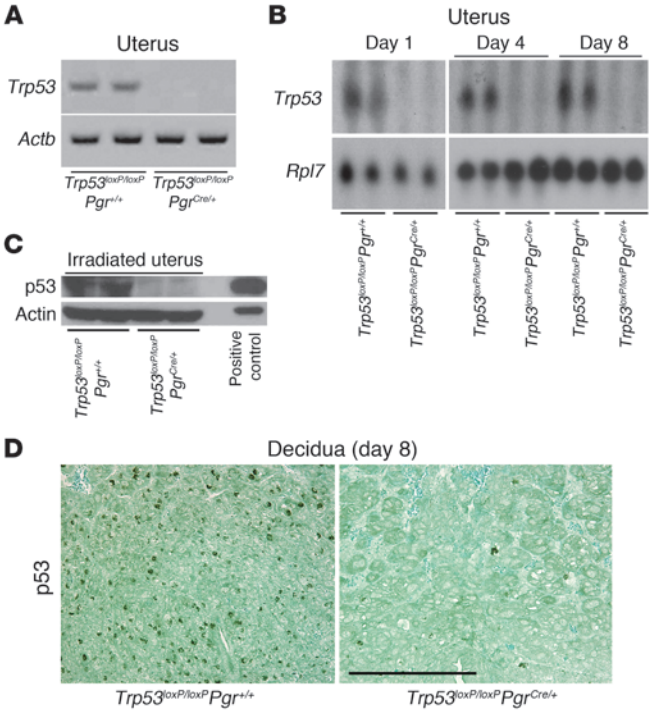

Figure 1
Efficient deletion of uterine *Trp53*. (**A** and **B**) *Trp53* mRNA was undetectable in 2-month-old *Trp53*$^{loxP/loxP}$*Pgr*$^{Cre/+}$ uteri analyzed by RT-PCR (**A**) and Northern hybridization (**B**). *Actb* and *Rpl7* were used as internal controls. (**C**) p53 protein levels were very low to undetectable in irradiation-induced 2-month-old *Trp53*$^{loxP/loxP}$*Pgr*$^{Cre/+}$ uteri assessed by Western blotting. *Trp53*$^{loxP/loxP}$*Pgr*$^{+/+}$ and *Trp53*$^{loxP/loxP}$*Pgr*$^{Cre/+}$ dams were killed 6 hours after 9.5 Gy whole-body γ irradiation. Protein extracts from mouse lymphoma cell line WR19L were used as a positive control. (**D**) Immunostaining of p53 in *Trp53*$^{loxP/loxP}$*Pgr*$^{+/+}$ and *Trp53*$^{loxP/loxP}$*Pgr*$^{Cre/+}$ decidua on day 8 of pregnancy. Immunoreactive p53 was undetectable in *Trp53*$^{loxP/loxP}$*Pgr*$^{Cre/+}$ decidua. Fast Green solution was used to counterstain the cytoplasm. Dark green-black staining shows nuclear p53 localization. Scale bar: 200 μm.

pathway evoked premature birth. These results unravel what we believe to be a new role of p53 in parturition.

Results

Trp53 is efficiently deleted in uteri of Trp53$^{loxP/loxP}$*Pgr*$^{Cre/+}$ *females*. We generated *Trp53*$^{loxP/loxP}$*Pgr*$^{Cre/+}$ and *Trp53*$^{loxP/loxP}$*Pgr*$^{+/+}$ mice by crossing *Trp53*$^{loxP/loxP}$ mice (FVB/129) with *Pgr*$^{Cre/+}$ mice (C57BL6/129) to examine various events during pregnancy (see Methods). Throughout the present study, we used littermate females to compare reproductive functions between control and experimental groups to minimize the influence of genetic background on the observed phenotypes. *Pgr*$^{Cre/+}$ females have been reported to have normal fertility (11). By breeding WT or *Pgr*$^{Cre/+}$ females with *Pgr*$^{Cre/+}$ males, we also confirmed that these females were fertile with normal gestational length (Supplemental Figure 1; supplemental material available online with this article; doi:10.1172/JCI40051DS1). In addition, we found that heterozygous floxed *Trp53* females with (*Trp53*$^{loxP/+}$*Pgr*$^{Cre/+}$) or without (*Trp53*$^{loxP/+}$*Pgr*$^{+/+}$) a *PR*-Cre allele on a mixed background had normal pregnancy outcome (Table 1). Therefore, PR haploinsufficiency or the presence of Cre did not show any adverse effect on pregnancy outcome. This is consistent with the findings of similar PR expression patterns in *Trp53*$^{loxP/loxP}$*Pgr*$^{+/+}$ and *Trp53*$^{loxP/loxP}$*Pgr*$^{Cre/+}$ pregnant uteri (Supplemental Figure 2). With these results in hand, we used 2-month-old littermate *Trp53*$^{loxP/loxP}$*Pgr*$^{+/+}$ and *Trp53*$^{loxP/loxP}$*Pgr*$^{Cre/+}$ dams on a mixed background to examine various reproductive events during pregnancy. We first confirmed that these dams had efficient deletion of uterine *Trp53* (Figure 1, A–D), with no sign of tumorigenesis in the uterus or other organs as we previously reported (12), as opposed to that found in mice with global deletion of *Trp53* (7).

Ovulation, fertilization, preimplantation development, and implantation are normal in Trp53$^{loxP/loxP}$*Pgr*$^{Cre/+}$ *dams*. We examined ovulation and fertilization in *Trp53*$^{loxP/loxP}$*Pgr*$^{Cre/+}$ dams by flushing eggs and/or embryos on day 2 of pregnancy and found both processes to be normal (Supplemental Figure 3, A and B). We also confirmed normal development of preimplantation embryos and their timely transport from the oviduct into uterine lumens of *Trp53*$^{loxP/loxP}$*Pgr*$^{Cre/+}$ dams by recording the number of blastocysts retrieved in uterine flushings on day 4 of pregnancy (Supplemental Figure 3C).

Table 1
Trp53$^{loxP/loxP}$*Pgr*$^{Cre/+}$ mice exhibit preterm birth and dystocia

Dam genotype	Day of labor	No. dams	No. dams with dystocia	No. dead pups per dam	No. live pups per dam
Trp53$^{loxP/+}$*Pgr*$^{+/+}$	Day 19, 1800 h, to day 20, 0800 h	8	0 (0%)	0.4 ± 0.3	8.4 ± 1.0
Trp53$^{loxP/+}$*Pgr*$^{Cre/+}$	Day 19, 1800 h, to day 20, 0800 h	8	0 (0%)	0.1 ± 0.1	8.5 ± 0.7
Trp53$^{loxP/loxP}$*Pgr*$^{+/+}$	Day 19, 0800 h, to day 19, 1800 h	2	0 (0%)	0.5 ± 0.5	10.5 ± 0.5
Trp53$^{loxP/loxP}$*Pgr*$^{+/+}$	Day 19, 1800 h, to day 20, 0800 h	21	0 (0%)	0.2 ± 0.1	9.3 ± 0.4
Trp53$^{loxP/loxP}$*Pgr*$^{+/+}$	Total	23	0 (0%)	0.2 ± 0.1	9.4 ± 0.5
Trp53$^{loxP/loxP}$*Pgr*$^{Cre/+}$	Day 17, 1200 h, to day 17, 1800 h	3	3 (100%)	7.0 ± 1.5	2.7 ± 2.7
Trp53$^{loxP/loxP}$*Pgr*$^{Cre/+}$	Day 17, 1800 h, to day 18, 1800 h	9	6 (67%)	5.0 ± 0.5	1.8 ± 0.8
Trp53$^{loxP/loxP}$*Pgr*$^{Cre/+}$	Day 18, 1800 h, to day 19, 1800 h	5	2 (40%)	0.8 ± 0.4	8.2 ± 0.7
Trp53$^{loxP/loxP}$*Pgr*$^{Cre/+}$	Day 19, 1800 h, to day 20, 0800 h	3	0 (0%)	0.7 ± 0.7	8.3 ± 1.2
Trp53$^{loxP/loxP}$*Pgr*$^{Cre/+}$	Day 20, 0800 h, to day 21, 0800 h	3	0 (0%)	1.3 ± 0.9	4.7 ± 2.3
Trp53$^{loxP/loxP}$*Pgr*$^{Cre/+}$	Total	23	11 (48%)	3.3 ± 0.6^{A}	4.5 ± 0.8^{A}

Littermate *Trp53*$^{loxP/+}$*Pgr*$^{+/+}$ and *Trp53*$^{loxP/+}$*Pgr*$^{Cre/+}$ dams (F1 generation) and littermate *Trp53*$^{loxP/loxP}$*Pgr*$^{+/+}$ and *Trp53*$^{loxP/loxP}$*Pgr*$^{Cre/+}$ dams (F3 generation) were used (see Methods). Day of labor was defined as the day of pregnancy when the dam delivers the first pup. Dystocia was defined as difficult delivery lasting more than 12 hours. The number of dead or live pups per dam is shown as mean ± SEM. $^{A}P < 0.05$ versus *Trp53*$^{loxP/loxP}$*Pgr*$^{+/+}$ dams; Student's *t* test.

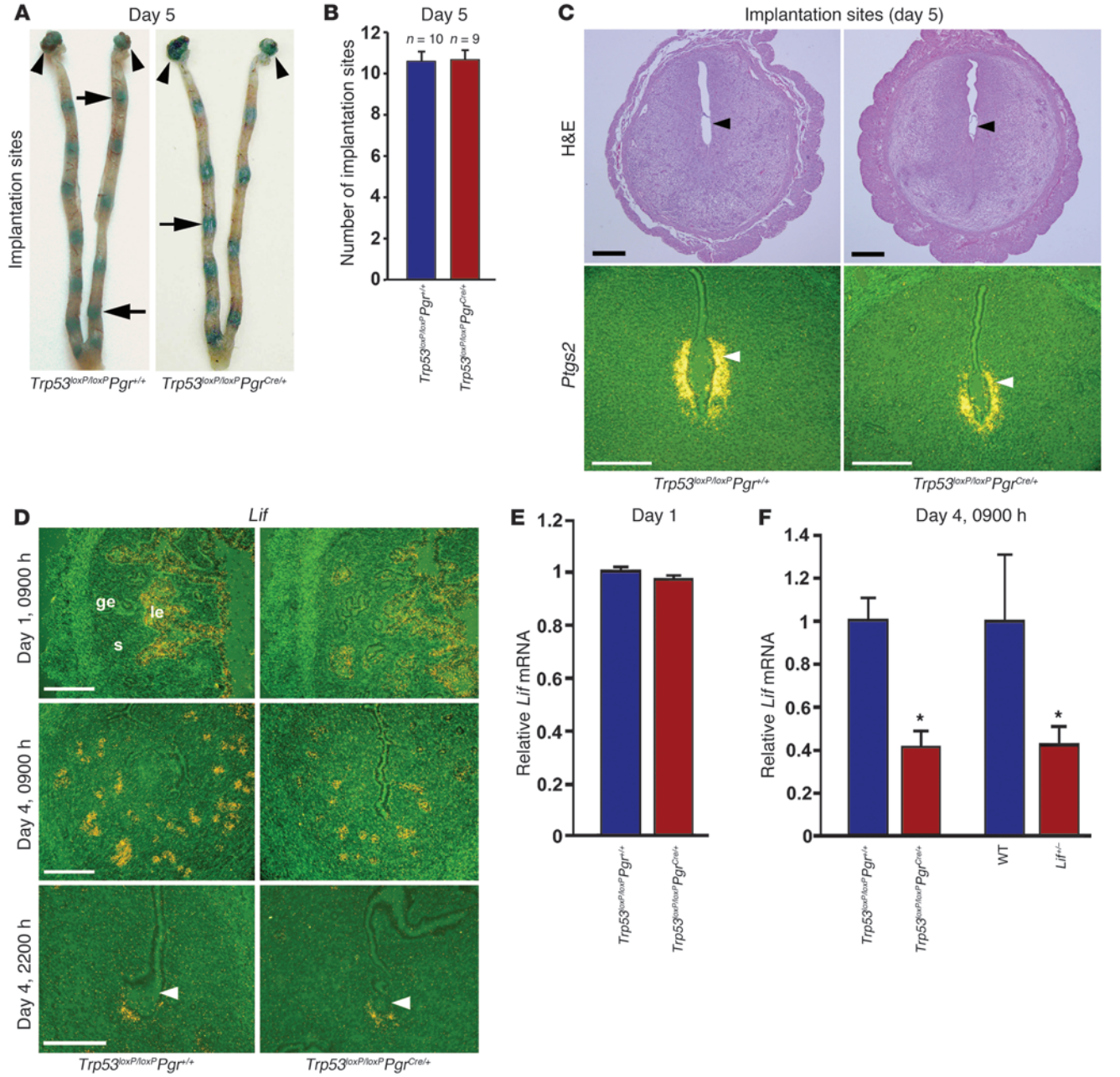

Figure 2

Mice with uterine deletion of *Trp53* show normal implantation. (**A**) Representative photographs of uteri with implantation sites (blue bands) on day 5 of pregnancy in $Trp53^{loxP/loxP}Pgr^{+/+}$ and $Trp53^{loxP/loxP}Pgr^{Cre/+}$ females, mated with fertile $Trp53^{loxP/loxP}Pgr^{+/+}$ males. Arrows and arrowheads indicate implantation sites and ovaries, respectively. (**B**) Number of implantation sites on day 5 of pregnancy (mean ± SEM; $P > 0.05$; Student's *t* test). (**C**) Representative photomicrographs of H&E-stained histology, and in situ hybridization of *Ptgs2*, in implantation sites on day 5 of pregnancy in $Trp53^{loxP/loxP}Pgr^{+/+}$ and $Trp53^{loxP/loxP}Pgr^{Cre/+}$ dams. Arrowheads indicate the location of implanting blastocysts. Scale bars: 200 μm. (**D**) In situ hybridization of *Lif* in $Trp53^{loxP/loxP}Pgr^{+/+}$ and $Trp53^{loxP/loxP}Pgr^{Cre/+}$ uterine sections on days 1 and 4 of pregnancy. Scale bars: 200 μm. (**E** and **F**) *Lif* mRNA levels in day 1 uteri of $Trp53^{loxP/loxP}Pgr^{+/+}$ and $Trp53^{loxP/loxP}Pgr^{Cre/+}$ dams (**E**) and in day 4, 0900 h, uteri of $Trp53^{loxP/loxP}Pgr^{+/+}$, $Trp53^{loxP/loxP}Pgr^{Cre/+}$, WT, and $Lif^{+/-}$ dams (**F**), as determined by Northern hybridization. Values are mean ± SEM of 2–4 independent samples. *$P < 0.05$, Student's *t* tests.

Successful implantation is the result of reciprocal interactions between the blastocyst and the receptive uterus. The receptive state of the uterus is transient and is defined as the time at which the uterine environment is conducive to blastocyst acceptance and implantation. In mice, generalized stromal edema late on the morning of day 4 leads to uterine luminal closure, placing the blastocyst in close apposition with the luminal epithelium. This is followed by an intimate adherence of the blastocyst trophectoderm with the luminal epithelium (attachment reaction), marking the first discernible sign of implantation on the night of day 4,

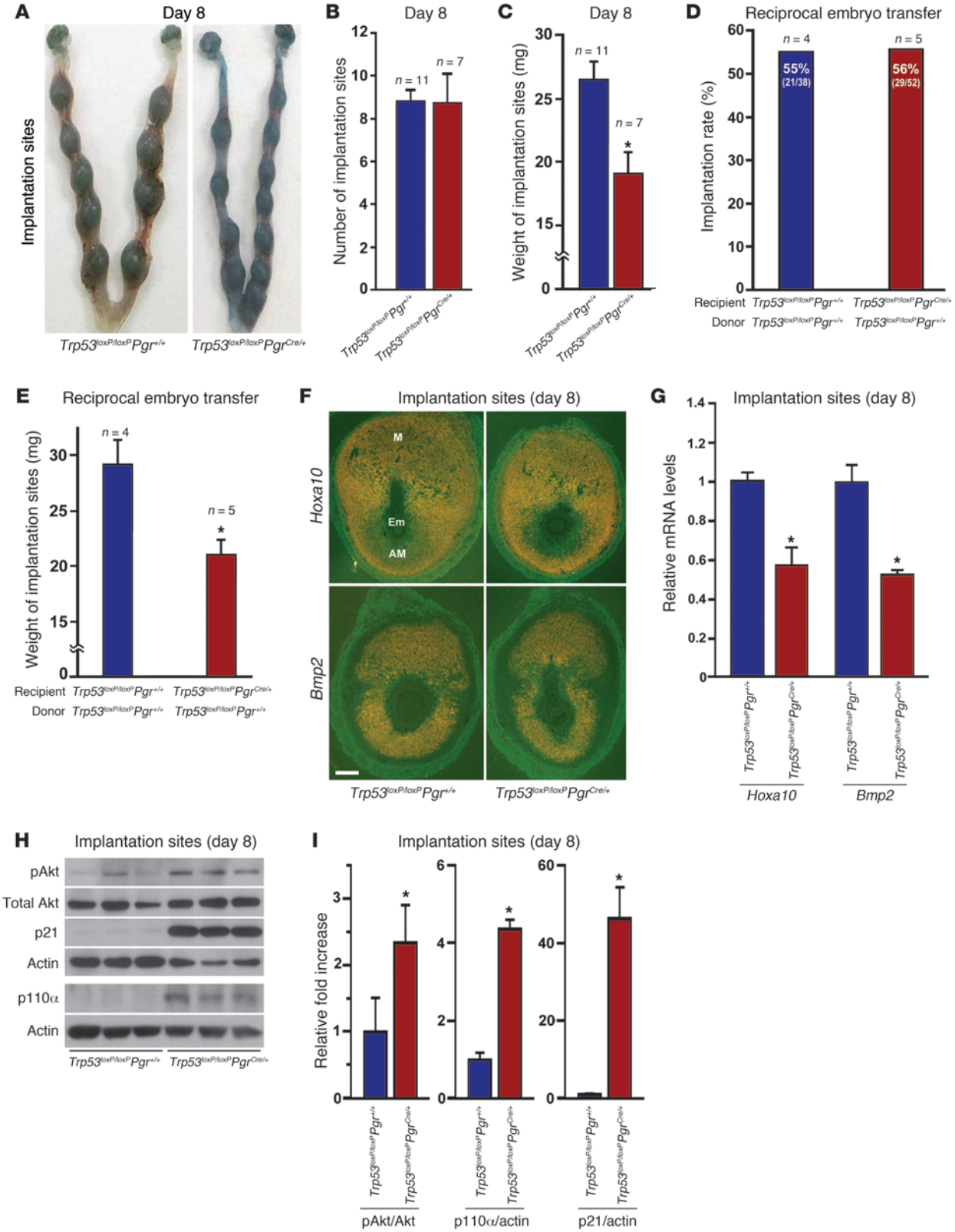
A
Day 8
Implantation sites
Trp53loxP/loxPPgr+/+
Trp53loxP/loxPPgrCre/+
B
Day 8
Number of implantation sites
n = 11
n = 7
C
Day 8
Weight of implantation sites (mg)
n = 11
n = 7
*
D
Reciprocal embryo transfer
Implantation rate (%)
n = 4
55%
(21/38)
n = 5
56%
(29/52)
Recipient Trp53loxP/loxPPgr+/+ Trp53loxP/loxPPgrCre/+
Donor Trp53loxP/loxPPgr+/+ Trp53loxP/loxPPgr+/+
E
Reciprocal embryo transfer
Weight of implantation sites (mg)
n = 4
n = 5
*
Recipient Trp53loxP/loxPPgr+/+ Trp53loxP/loxPPgrCre/+
Donor Trp53loxP/loxPPgr+/+ Trp53loxP/loxPPgr+/+
F
Implantation sites (day 8)
Hoxa10
Bmp2
M
Em
AM
Trp53loxP/loxPPgr+/+
Trp53loxP/loxPPgrCre/+
G
Implantation sites (day 8)
Relative mRNA levels
*
Hoxa10
Bmp2
H
Implantation sites (day 8)
pAkt
Total Akt
p21
Actin
p110α
Actin
Trp53loxP/loxPPgr+/+
Trp53loxP/loxPPgrCre/+
I
Implantation sites (day 8)
Relative fold increase
*
pAkt/Akt
p110α/actin
p21/actin

Figure 3
Uterine deletion of *Trp53* restricts normal decidual growth. (**A**) Representative photographs of day 8 pregnant implantation sites in *Trp53*$^{loxP/loxP}$*Pgr*$^{+/+}$ and *Trp53*$^{loxP/loxP}$*Pgr*$^{Cre/+}$ mice. (**B** and **C**) Number and weight of implantation sites in *Trp53*$^{loxP/loxP}$*Pgr*$^{+/+}$ and *Trp53*$^{loxP/loxP}$*Pgr*$^{Cre/+}$ mice on day 8 of pregnancy (mean ± SEM; **P* < 0.05). (**D** and **E**) *Trp53*$^{loxP/loxP}$*Pgr*$^{+/+}$ blastocysts were transferred into uteri of *Trp53*$^{loxP/loxP}$*Pgr*$^{+/+}$ or *Trp53*$^{loxP/loxP}$*Pgr*$^{Cre/+}$ recipients on day 4 of pseudopregnancy. The number and weight of implantation sites were evaluated on day 8, 4 days after embryo transfer (mean ± SEM; **P* < 0.05). Numbers in parentheses denote the ratio of implantation sites/total blastocysts transferred. (**F**) In situ hybridization of *Hoxa10* and *Bmp2* in *Trp53*$^{loxP/loxP}$*Pgr*$^{+/+}$ and *Trp53*$^{loxP/loxP}$*Pgr*$^{Cre/+}$ uteri on day 8 of pregnancy. Em, embryo; M, mesometrial pole; AM, antimesometrial pole. Scale bar: 200 μm. (**G**) Northern hybridization of *Hoxa10* and *Bmp2* in day 8 uteri of *Trp53*$^{loxP/loxP}$*Pgr*$^{+/+}$ and *Trp53*$^{loxP/loxP}$*Pgr*$^{Cre/+}$ dams. In each group, 2–3 independent samples were examined (mean ± SEM; **P* < 0.05). (**H** and **I**) Loss of p53 upregulated pAkt, p110α, and p21 levels in day 8 implantation sites. As assessed by Western blotting (**H**), quantitatively analyzed band intensities of pAkt were normalized against total Akt, and those of p110α and p21 were normalized against actin (**I**). In each group, 3 independent samples from different mice were examined (mean ± SEM; **P* < 0.05).

between 2200 h and 2400 h. The attachment reaction coincides with increased stromal vascular permeability at the site of the blastocyst and can be demarcated by distinct blue bands along the uterus after intravenous injection of a blue dye solution (13). We found that *Trp53*$^{loxP/loxP}$*Pgr*$^{Cre/+}$ dams had numbers of distinct implantation sites comparable to those of *Trp53*$^{loxP/loxP}$*Pgr*$^{+/+}$ dams on the night of day 4 (data not shown). The implantation process in progress was also normal in *Trp53*$^{loxP/loxP}$*Pgr*$^{Cre/+}$ dams on day 5 of pregnancy, as assessed by the blue dye method and histological analysis (Figure 2, A–C). COX2, encoded by *Ptgs2*, is an inducible rate-limiting enzyme required for the biosynthesis of prostaglandins (PGs). COX2 is expressed in the luminal epithelium and stroma exclusively at the site of blastocyst attachment and is critical for implantation (14). We found that expression patterns of *Ptgs2* mRNA and COX2 protein were similar between *Trp53*$^{loxP/loxP}$*Pgr*$^{+/+}$ and *Trp53*$^{loxP/loxP}$*Pgr*$^{Cre/+}$ dams during implantation (Figure 2C and Supplemental Figure 4).

Lif, an estrogen response gene, is required for uterine receptivity and implantation (15). It is first expressed in uterine glands on the morning of day 4, then in the stroma surrounding the blastocyst at the time of the attachment reaction the night of day 4, persisting through the morning of day 5 (16). Because reduced uterine *Lif* expression was previously reported to be the cause of implantation failure in *Trp53*$^{-/-}$ dams (6), we compared uterine *Lif* expression between *Trp53*$^{loxP/loxP}$*Pgr*$^{+/+}$ and *Trp53*$^{loxP/loxP}$*Pgr*$^{Cre/+}$ dams on days 1 and 4 of pregnancy and found their expression patterns to be similar (Figure 2D). We also found comparable levels of uterine *Lif* expression in *Trp53*$^{loxP/loxP}$*Pgr*$^{+/+}$ and *Trp53*$^{loxP/loxP}$*Pgr*$^{Cre/+}$ dams on day 1 (Figure 2E), when the uterus is under the influence of preovulatory estrogen surge, as well as in ovariectomized uteri after estrogen treatment (Supplemental Figure 5). However, similar to the previous report (6), we found about 60% reduction in *Lif* expression levels in *Trp53*$^{loxP/loxP}$*Pgr*$^{Cre/+}$ uteri on the morning of day 4, although these levels were comparable to those in *Lif*$^{+/-}$ dams (Figure 2F), which showed normal implantation and pregnancy (Supplemental Figure 6 and refs. 16, 17). Because reduced uterine *Lif* expression sustained normal pregnancy in *Lif*$^{+/-}$ mice, we believe that a similar reduction in uterine *Lif* expression in *Trp53*$^{loxP/loxP}$*Pgr*$^{Cre/+}$ mice would fail to prevent implantation. Furthermore, the stromal *Lif* expression pattern surrounding the blastocyst at the time of attachment on the night of day 4, also considered important for implantation (16, 17), was normal in *Trp53*$^{loxP/loxP}$*Pgr*$^{Cre/+}$ dams (Figure 2D). These findings show that reduced *Lif* expression levels in *Trp53*-deleted uteri on the morning of day 4 were not a limiting factor for implantation to occur, although this reduction could be detrimental to implantation in other conditions, as reported by Hu et al. (6). Because the expression of *Trp53* is primarily restricted to the stroma prior to and during implantation (18), and because the stroma can influence epithelial phenotypes (19), it is possible that some reduction in *Lif* expression levels on day 4 is secondary to stromal deficiency of p53 in *Trp53*$^{loxP/loxP}$*Pgr*$^{Cre/+}$ mice.

Deletion of uterine Trp53 leads to decidual growth restriction with polyploidy, terminal differentiation, and senescence. With the implantation process in progress, stromal cells surrounding the implanting embryo undergo decidualization, which is essential for sustaining pregnancy. To determine whether this process is normal in *Trp53*$^{loxP/loxP}$*Pgr*$^{Cre/+}$ dams, we first recorded weights of implantation sites in *Trp53*$^{loxP/loxP}$*Pgr*$^{+/+}$ and *Trp53*$^{loxP/loxP}$*Pgr*$^{Cre/+}$ dams on day 8 of pregnancy, the day of maximal decidual growth. The number of sites remained comparable between the 2 groups (Figure 3, A and B), but weights of implantation sites were lower in *Trp53*$^{loxP/loxP}$*Pgr*$^{Cre/+}$ dams (Figure 3, A and C), suggestive of alteration in decidual cell growth. To circumvent any effects of embryo genotype on implantation or decidualization, we performed reciprocal blastocyst transfer experiments. Day 4 *Trp53*$^{loxP/loxP}$*Pgr*$^{+/+}$ blastocysts were transferred into uteri of *Trp53*$^{loxP/loxP}$*Pgr*$^{+/+}$ or *Trp53*$^{loxP/loxP}$*Pgr*$^{Cre/+}$ recipients on day 4 of pseudopregnancy. Again, implantation rates were comparable between *Trp53*$^{loxP/loxP}$*Pgr*$^{+/+}$ and *Trp53*$^{loxP/loxP}$*Pgr*$^{Cre/+}$ recipient dams (Figure 3D), although weights of implantation sites were lower in *Trp53*$^{loxP/loxP}$*Pgr*$^{Cre/+}$ recipients (Figure 3E), on day 8 of pregnancy. *Hoxa10* and *Bmp2* are highly expressed in decidual cells and critical for decidualization (20–22). Expression patterns of *Hoxa10* and *Bmp2* in decidual cells surrounding the implanting blastocysts in *Trp53*$^{loxP/loxP}$*Pgr*$^{Cre/+}$ dams were similar to those in *Trp53*$^{loxP/loxP}$*Pgr*$^{+/+}$ dams (Figure 3F), although their expression levels were about 40% lower in *Trp53*$^{loxP/loxP}$*Pgr*$^{Cre/+}$ mice on day 8 (Figure 3G). Together, these findings suggested a role for uterine p53 in normal decidual growth and led us to explore the mechanism by which uterine p53 deficiency limits decidual growth.

Heightened stromal cell proliferation, differentiation, and polyploidy are hallmarks of normal decidualization in mice; alteration in any of these processes may influence decidual growth. One major role of the deciduum is to accommodate and support the developing embryo. It was previously shown using an in vitro model of human decidualization that withdrawal of decidualization stimuli downregulates p53, but induces Akt activation (23, 24). We also found increased levels of pAkt in implantation sites of *Trp53*$^{loxP/loxP}$*Pgr*$^{Cre/+}$ mice on day 8 of pregnancy (Figure 3, H and I). These increased levels were consistent with immunostained pAkt-positive decidual cells in *Trp53*$^{loxP/loxP}$*Pgr*$^{Cre/+}$ dams (data not shown). We also found increased levels of p110α, a catalytic subunit of PI3K, in the *Trp53*$^{loxP/loxP}$*Pgr*$^{Cre/+}$ mice (Figure 3, H and I). A recent study shows that *PIK3CA*, which encodes p110α, has 2 alternate promoters, and p53 binds directly to one of them to inhibit its transcription (25). In contrast, inactivation of p53 upregulates *PIK3CA*, resulting in enhanced PI3K activity with

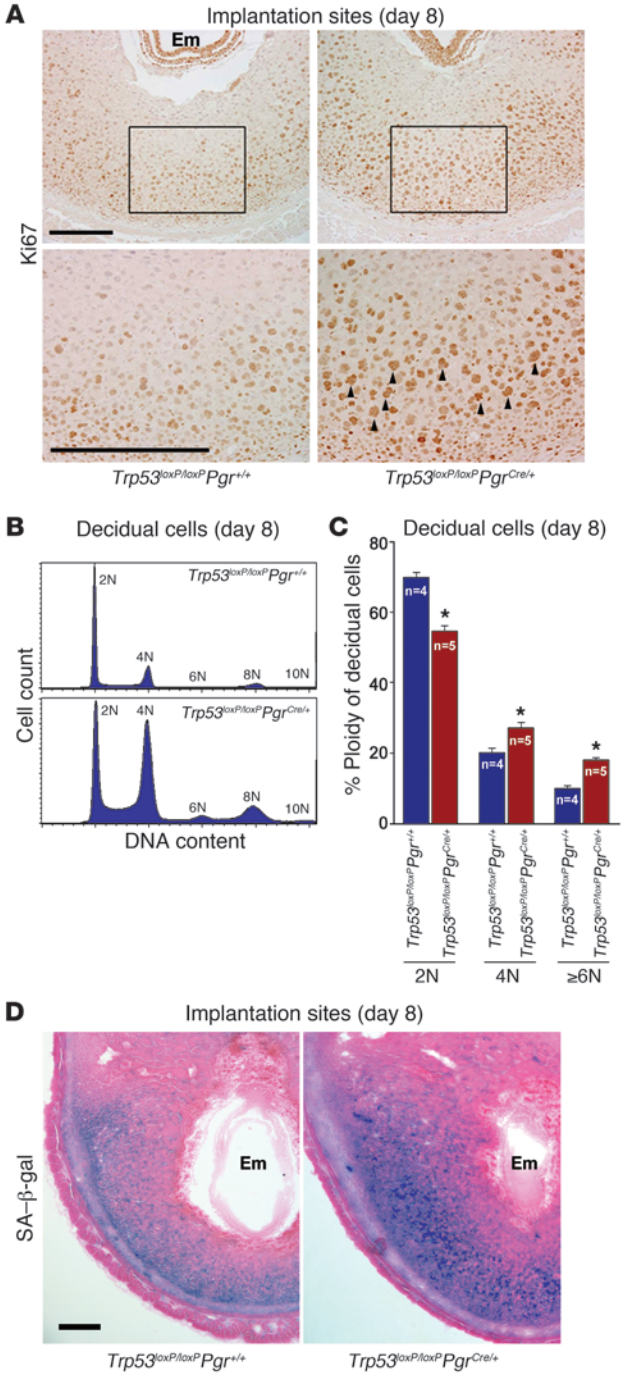

Figure 4
Uterine deletion of *Trp53* confers decidual polyploidy, terminal differentiation, and senescence. (**A**) Uterine loss of p53 increased Ki67-positive decidual cells with large nuclei. Higher-magnification views of the boxed regions are shown below. Arrowheads indicate Ki67-positive cells with large, irregularly shaped nuclei. Scale bars: 200 μm. (**B**) Representative histogram of flow cytometry analyses showing DNA content (propidium iodide). Ploidy is denoted by -N (i.e., 2N, diploid; 4N–10N, polyploid). (**C**) In $Trp53^{loxP/loxP}Pgr^{Cre/+}$ decidua, the number of diploid cells decreased, whereas the number of polyploid cells increased (mean ± SEM; $^*P < 0.05$, Student's *t* tests). (**D**) Uterine *Trp53* deletion enhanced SA–β-gal activity in decidua. Scale bar: 200 μm.

increased levels of pAkt (25). Therefore, our observations of increased levels of p110α and pAkt provide evidence that conditional deletion of *Trp53* in the uterus stimulates PI3K activity, which in turn elevates pAkt levels.

We also found heightened expression of p21, a cyclin-dependent kinase inhibitor (Figure 3, H and I). Normally, p21 is transcriptionally upregulated by p53 after DNA damage. However, p21 is also induced independently of p53 in multiple cell lineages with terminal differentiation during tissue development (26, 27). In this respect, the function of p53 in developing tissues is different from its role in adult tissues. Since the growing deciduum is a maternal counterpart during embryo development, the roles of p53 and its targets in decidua may be similar to those in developing embryos. Stromal cells often enter the endoreplication cycle and become polyploid with p21 expression during normal decidual differentiation (28); therefore, the upregulation of p21 in $Trp53^{loxP/loxP}Pgr^{Cre/+}$ uteri suggests that p53 deficiency stimulates decidual polyploidy, favoring terminal cell differentiation. In fact, we found numerous Ki67-positive decidual cells with large, irregularly shaped nuclei in $Trp53^{loxP/loxP}Pgr^{Cre/+}$ dams (Figure 4A), and flow cytometry analysis confirmed substantial increases in decidual cells with a DNA complement higher than 2N in $Trp53^{loxP/loxP}Pgr^{Cre/+}$ dams on day 8 of pregnancy (Figure 4, B and C). Taken together, these results provide evidence that uterine loss of p53 enhances the endoreplication cycle, ultimately pushing decidual cells toward terminal differentiation. Our findings are consistent with previous findings of increased numbers of polyploid cells in pancreases of $Trp53^{-/-}$ pups (29), increased p21 expression in $Trp53^{-/-}$ megakaryocytes during polyploidization (30), and decreased *Trp53* expression with terminal differentiation of developing tissues (31). More interestingly, we found that enhanced terminal differentiation of decidua in $Trp53^{loxP/loxP}Pgr^{Cre/+}$ dams was associated with increased senescence-associated β-galactosidase (SA-β-gal) activity (Figure 4D), suggestive of senescence-induced decidual growth restriction, in $Trp53^{loxP/loxP}Pgr^{Cre/+}$ uteri. p21 is known to be a major contributor to senescence (32), and Akt activation also induces senescence (33). In addition, pAkt can enhance the stability of p21 protein through phosphorylation (34). Thus, upregulated p21 and pAkt levels are likely causes of senescence-induced decidual growth restriction in mice with uterine deletion of *Trp53*.

Deletion of uterine Trp53 promotes preterm delivery. Despite this decidual growth restriction, $Trp53^{loxP/loxP}Pgr^{Cre/+}$ mice did not show increased incidence of resorption or pregnancy loss even on day 16 of pregnancy (Figure 5A). However, as expected, implantation sites were smaller in $Trp53^{loxP/loxP}Pgr^{Cre/+}$ dams (Figure 5B). Our observation of positive cytokeratin staining in the placenta, but its absence in the deciduum, clearly showed that decidual areas were smaller in $Trp53^{loxP/loxP}Pgr^{Cre/+}$ dams compared with $Trp53^{loxP/loxP}Pgr^{+/+}$ dams (Figure 5C), suggestive of reduced decidual growth and thickness. The weights of both embryos and placentas were also low in $Trp53^{loxP/loxP}Pgr^{Cre/+}$ mice, despite comparable ratios of fetal to placental weight (Supplemental Figure 7). More interestingly, we found that increased SA–β-gal activity was sustained in the decidual layer on days 12 and 16 (Figure 5D), and that levels of p21, a senescence-associated marker (32, 35), were also upregulated in $Trp53^{loxP/loxP}Pgr^{Cre/+}$ uteri on day 16 (Figure 5, E and F). These findings suggest premature uterine senescence in $Trp53^{loxP/loxP}Pgr^{Cre/+}$ dams during pregnancy. Alterations in decidual

growth and SA–β-gal activity (data not shown) or placental and fetal weights (Supplemental Figure 8A) in *Trp53*$^{loxP/loxP}$*Pgr*$^{Cre/+}$ dams were independent of embryonic genotypes. In addition, SA–β-gal activity was undetectable in fetuses or placentas (data not shown). In parallel to heightened p21 levels, pAkt levels were also higher in *Trp53*$^{loxP/loxP}$*Pgr*$^{Cre/+}$ uteri, probably resulting from increased PI3K activity caused by upregulated p110α in these mice (Figure 5, E and F). This was reflected in increased signals of pAkt immunostaining in *Trp53*$^{loxP/loxP}$*Pgr*$^{Cre/+}$ decidua (Supplemental Figure 9). These findings suggest that p21 and pAkt cooperatively promote premature decidual senescence and growth restriction that in turn affect fetoplacental growth in *Trp53*$^{loxP/loxP}$*Pgr*$^{Cre/+}$ dams. However, CD31-positve cells in the decidual vascular bed were comparable between *Trp53*$^{loxP/loxP}$*Pgr*$^{+/+}$ and *Trp53*$^{loxP/loxP}$*Pgr*$^{Cre/+}$ dams on day 16 (Supplemental Figure 9).

Because ovarian hormones are known to influence pregnancy events, including decidual growth, parturition, and pregnancy outcome (36), we measured serum estradiol-17β (E_2) and P_4 levels in *Trp53*$^{loxP/loxP}$*Pgr*$^{+/+}$ and *Trp53*$^{loxP/loxP}$*Pgr*$^{Cre/+}$ dams at critical time points during pregnancy found them to be comparable between groups (Figure 5G). These hormone levels were consistent with functional corpora lutea with low and comparable levels of 20α–hydroxysteroid dehydrogenase (20α-HSD) in *Trp53*$^{loxP/loxP}$*Pgr*$^{+/+}$ and *Trp53*$^{loxP/loxP}$*Pgr*$^{Cre/+}$ dams on day 16 of pregnancy (Figure 5, H–J). This enzyme converts P_4 to an inactive metabolite and is a known marker of luteolysis (37).

Although restricted decidual growth did not enhance the rate of resorption, a surprising event occurred: the incidence of premature birth significantly increased in *Trp53*$^{loxP/loxP}$*Pgr*$^{Cre/+}$ dams (Figure 6A). Specifically, whereas all *Trp53*$^{loxP/loxP}$*Pgr*$^{+/+}$ dams experienced labor late on day 19 or early on day 20 with viable offspring, more than 50% of *Trp53*$^{loxP/loxP}$*Pgr*$^{Cre/+}$ dams delivered on days 17 or 18 (Table 1), with 100% of newborn pups dying during labor or just after birth (Figure 6B). Furthermore, 75% of *Trp53*$^{loxP/loxP}$*Pgr*$^{Cre/+}$ dams with preterm birth (9 of 12) showed signs of dystocia, with prolonged labor over a period of 12 hours (Table 1). The phenotype of preterm delivery was also observed in *Trp53*$^{loxP/loxP}$*Pgr*$^{Cre/+}$ dams on a CD1 background (Supplemental Figure 10), which suggests that this phenotype is not restricted to a specific genetic background. These findings led us to explore the underlying mechanism that triggers premature birth.

Deletion of uterine Trp53 provokes preterm delivery via the pAkt/COX2 pathway. In many species, PGs such as PGE_2 and $PGF_{2\alpha}$ participate in labor as contractile mediators (38). The COX enzymes, COX1 and COX2, catalyze the rate-limiting step in PG biosynthesis from arachidonic acid (39). COX1 and COX2 convert arachidonic acid to PGH_2, which is subsequently converted to $PGF_{2\alpha}$, PGE_2, and PGI_2 by PGF synthase (PGFS), microsomal PGE synthase–1 (mPGES1, encoded by *Ptges1*), and PGI synthase (PGIS, encoded by *Ptgis*), respectively (40). COX1-derived PGs are known to influence parturition in mice (41). However, to our surprise, levels of uterine COX1 remained unaltered in *Trp53*$^{loxP/loxP}$*Pgr*$^{+/+}$ and *Trp53*$^{loxP/loxP}$*Pgr*$^{Cre/+}$ dams on day 16 (Figure 6, C and D). Instead, levels of COX2 were elevated in *Trp53*$^{loxP/loxP}$*Pgr*$^{Cre/+}$ uteri compared with those in *Trp53*$^{loxP/loxP}$*Pgr*$^{+/+}$ uteri on day 16 (Figure 6, C and D). It is highly probable that increased levels of COX2-derived PGs initiated the early onset of labor in *Trp53*$^{loxP/loxP}$*Pgr*$^{Cre/+}$ dams in the face of unaltered COX1 levels. Indeed, levels of $PGF_{2\alpha}$, but not other PGs, were significantly upregulated in *Trp53*-deleted uteri on day 16 of pregnancy (Figure 6E). Higher uterine $PGF_{2\alpha}$ levels in *Trp53*$^{loxP/loxP}$*Pgr*$^{Cre/+}$ dams were independent of embryo genotypes (Supplemental Figure 8B). This upregulation is consistent with selective increases of liver- and lung-type PGFS in *Trp53*$^{loxP/loxP}$*Pgr*$^{Cre/+}$ compared with *Trp53*$^{loxP/loxP}$*Pgr*$^{+/+}$ dams on day 16 (Figure 6, C and D). However, whereas levels of *Ptges1* were lower in *Trp53*$^{loxP/loxP}$*Pgr*$^{Cre/+}$ uteri, levels of *Ptgis* and *Hpgd* (encoding 15-hydroxyprostaglandin dehydrogenase; 15-HPGD) were not appreciably different (Supplemental Figure 11). It is known that liver- and lung-type PGFSs are highly expressed in the mouse uterus just prior to parturition (42). $PGF_{2\alpha}$ is known to play an important role in the initiation of parturition in mice (43). Studies in mice with deletion of PGF receptor FP (*Ptgfr*$^{-/-}$) show that $PGF_{2\alpha}$ acts on ovarian FP receptors to induce luteolysis, leading to the fall in P_4 levels required for triggering labor (44). PGE_2 and $PGF_{2\alpha}$ are primarily metabolized by 15-HPGD (45, 46), and mice carrying 15-HPGD hypomorphic alleles show spontaneous preterm labor with increased levels of $PGF_{2\alpha}$ in the absence of luteolysis and P_4 withdrawal (47). We observed similar circulating levels of E_2 and P_4 in *Trp53*$^{loxP/loxP}$*Pgr*$^{+/+}$ and *Trp53*$^{loxP/loxP}$*Pgr*$^{Cre/+}$ dams without luteolysis on day 16 (Figure 5, G–J), which suggests that the onset of preterm labor in *Trp53*$^{loxP/loxP}$*Pgr*$^{Cre/+}$ mice is caused by direct contractile effects of higher COX2-derived $PGF_{2\alpha}$ levels in the uterus, not by early luteolysis.

Oxytocin is uterotonic and acts via oxytocin receptor (OXTR; ref. 48), a contractile-associated protein that is upregulated during parturition (43). *Oxtr* is not induced in *Ptgfr*$^{-/-}$ uteri during parturition (44), which suggests that $PGF_{2\alpha}$ induces OXTR at the time of labor. Interestingly, mice deficient in oxytocin or OXTR apparently show normal parturition (49, 50), raising questions regarding the critical roles of oxytocin/OXTR signaling in parturition in mice. We found a 45% increase in *Oxtr* expression in *Trp53*$^{loxP/loxP}$*Pgr*$^{Cre/+}$ uteri on day 16 (Supplemental Figure 12A), which suggests that perhaps increased $PGF_{2\alpha}$ levels stimulated OXTR expression to complement contractile effects. Because activation of Akt induces COX2 in the mouse uterus (12), and because both COX2 and pAkt were clearly localized in *Trp53*$^{loxP/loxP}$*Pgr*$^{Cre/+}$ decidual cells (Supplemental Figure 9), it is highly likely that increased levels of uterine pAkt stimulate COX2-induced $PGF_{2\alpha}$ levels to initiate preterm labor. This is supported by the finding of reversal of preterm delivery and neonatal death in *Trp53*$^{loxP/loxP}$*Pgr*$^{Cre/+}$ dams by oral gavage of the selective COX2 inhibitor celecoxib on day 16 (Figure 6, F and G). Taken together, these findings reinforce that deletion of uterine p53 induces premature delivery via activation of the Akt/COX2/PGFS/$PGF_{2\alpha}$ signaling axis. Notably, cervical ripening was not evident in *Trp53*$^{loxP/loxP}$*Pgr*$^{Cre/+}$ dams on day 16 of pregnancy (Supplemental Figure 12B), in spite of heightened uterine $PGF_{2\alpha}$ levels. This suggests that preterm uterine contraction without cervical ripening contributed to dystocia in *Trp53*$^{loxP/loxP}$*Pgr*$^{Cre/+}$ dams.

Discussion

The highlight of the present study is that conditional deletion of uterine *Trp53* in mice promoted terminal differentiation of decidual cells and premature uterine senescence, leading to preterm birth with dystocia and neonatal death. Because pAkt and p21 are known to be involved in terminal cell differentiation and senescence in other systems (32, 33), their increased levels in the deciduum missing p53 are likely causes of these observed effects. In pursuit of the underlying cause of premature birth, we found persistent signs of increased decidual senescence with increased levels of pAkt and COX2. Because pAkt is known to upregulate

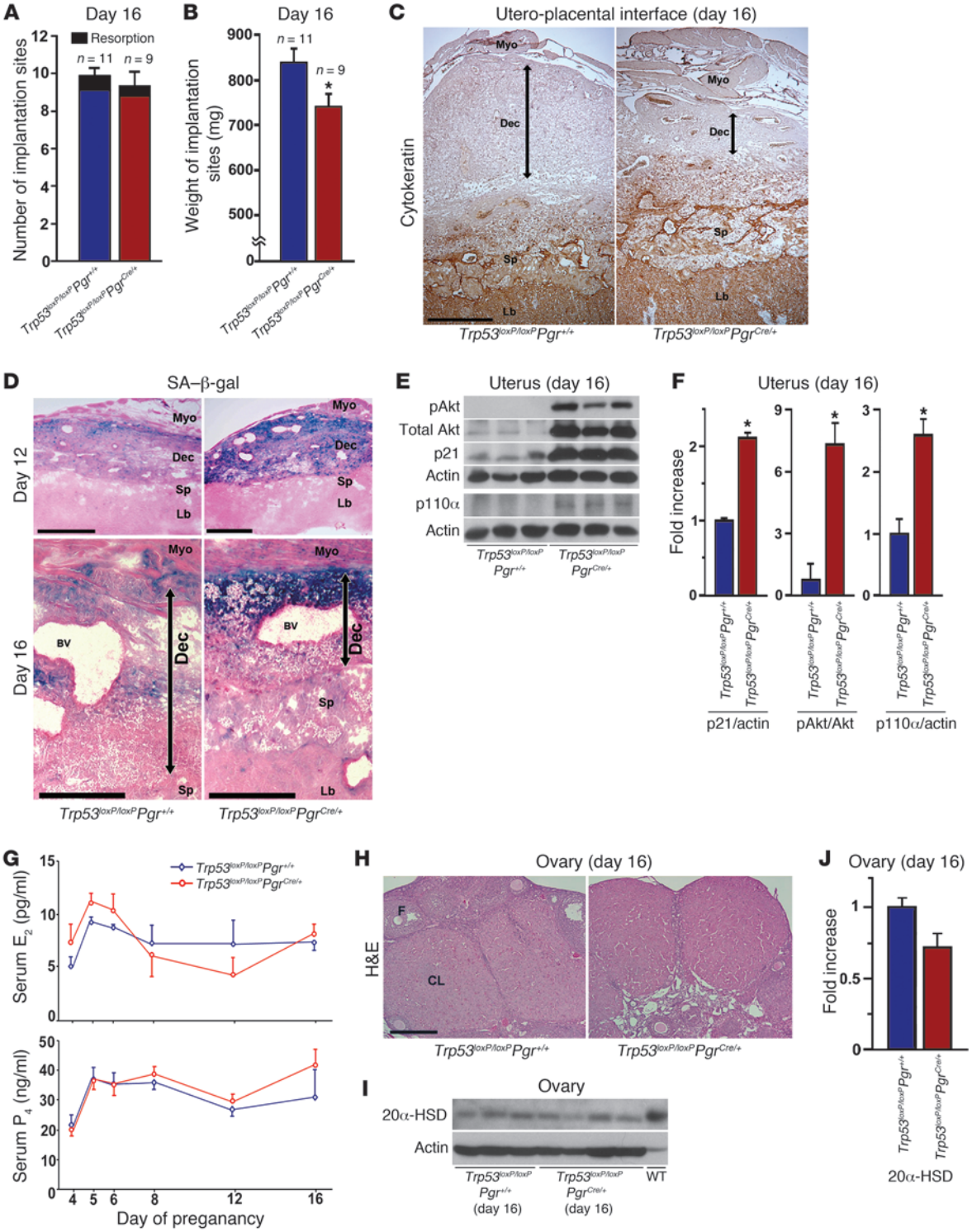
A
Day 16
Resorption
n = 11
n = 9
Number of implantation sites
Trp53loxP/loxPPgr+/+
Trp53loxP/loxPPgrCre/+
B
Day 16
n = 11
n = 9
*
Weight of implantation sites (mg)
C
Utero-placental interface (day 16)
Cytokeratin
Myo
Dec
Sp
Lb
D
SA–β-gal
Day 12
Day 16
BV
E
Uterus (day 16)
pAkt
Total Akt
p21
Actin
p110α
F
Uterus (day 16)
Fold increase
p21/actin
pAkt/Akt
p110α/actin
G
Serum E2 (pg/ml)
Serum P4 (ng/ml)
Day of preganancy
H
Ovary (day 16)
H&E
F
CL
I
Ovary
20α-HSD
WT
(day 16)
J
Ovary (day 16)
Fold increase
20α-HSD

Figure 5
Decidual senescence persists in uteri deleted of *Trp53*. (**A** and **B**) Number and weight of implantation sites in $Trp53^{loxP/loxP}Pgr^{+/+}$ and $Trp53^{loxP/loxP}Pgr^{Cre/+}$ mice on day 16 of pregnancy (mean ± SEM; $^*P < 0.05$). (**C**) Uterine loss of p53 impeded decidual growth. Placental labyrinth and spongiotrophoblast layers were demarcated by cytokeratin-8 immunostaining. (**D**) Uterine *Trp53* deletion enhanced SA–β-gal activity primarily in the decidual layer on days 12 and 16. (**C** and **D**) Decidual boundaries are demarcated by double-sided arrows. Myo, myometrium; Dec, decidua; Sp, spongiotrophoblast; Lb, labyrinth; BV, blood vessel. Scale bars: 500 μm. (**E** and **F**) Levels of p21, pAkt, and p110α were upregulated in day 16 uteri lacking p53. (**E**) Uterine samples from which placentas and fetuses had been removed were used for Western blotting. (**F**) Quantitative analysis of band intensities of pAkt were normalized against total Akt, and those of p21 and p110α were normalized against actin (mean ± SEM; $^*P < 0.05$). In each group, 3 independent samples from different mice were examined. (**G**) Serum levels of E_2 and P_4 (mean ± SEM; $P > 0.05$). At least 4 independent samples were examined in each group. (**H**) Representative photomicrographs of H&E-stained histological sections of ovaries on day 16 of pregnancy. CL, corpus luteum; F, follicle. Scale bar: 200 μm. (**I**) Western blotting of ovarian 20α-HSD levels on day 16 of pregnancy. Day-20 WT mice were used as a positive control. (**J**) Quantitative analysis of 20α-HSD band intensities from **I** were normalized against actin (mean ± SEM; $P > 0.05$).

COX2 levels in various cell types, including uterine cells (12), and because COX-derived PGs are crucial for the initiation of labor (38), we strongly believe that an early rise in uterine pAkt and COX2 levels initiated premature labor in $Trp53^{loxP/loxP}Pgr^{Cre/+}$ dams. Our conclusion was supported by the observation of increased uterine levels of PGFS and $PGF_{2\alpha}$ in the face of unaltered levels of COX1 and other PGs in these mice and the rescue of their preterm births by oral administration of celecoxib on day 16. Collectively, our results provide evidence that uterine deficiency of p53 evokes premature uterine senescence and elevates COX2-derived $PGF_{2\alpha}$ levels that cooperatively trigger preterm birth (Figure 7).

Our present observation is in contrast to the finding of only an implantation phenotype in $Trp53^{-/-}$ mice (6). The discrepancy between the prior study and our present one is likely due to different mouse models and/or experimental approaches used. However, the phenotype of difficult parturition in $Trp53^{-/-}$ females was previously reported in a review article as unpublished observations (51). Perhaps the parturition phenotype in $Trp53^{-/-}$ mice remained unnoticed for such a long time because most previous studies focused on tumorigenesis; however, this needs to be considered for future investigations using $Trp53^{-/-}$ females.

Lif, which is essential for implantation, is expressed in day 4 pregnant uteri at 2 different times (morning and night) in 2 different cell types (16). Our observation of reduced uterine *Lif* expression at similar levels on the morning of day 4 in both $Trp53^{loxP/loxP}Pgr^{Cre/+}$ and $Lif^{-/-}$ mice with normal implantation suggests that the mouse uterus is very sensitive to LIF. Thus, a lesser amount of LIF is sufficient for inducing implantation, similar to what was found for estrogen (52). After implantation, however, *Lif* expression is at low basal levels (53) and not required for pregnancy maintenance (54). In contrast, COX2 is expressed at several critical stages in a cell-specific manner during pregnancy. COX2 is expressed in the uterus not only at the time of blastocyst attachment (and is critical for this process; ref. 14), but also during decidualization and placentation, driving different functions. PGI_2 and PGE_2 are major PGs produced during implantation, decidualization, and placentation that participate in blastocyst attachment, trophoblast differentiation, and invasion via activation of the nuclear receptor PPARδ and/or the PGE_2 receptors EP2 and EP4 (55, 56). Our present study shows that although uterine levels of COX2 were very low in $Trp53^{loxP/loxP}Pgr^{+/+}$ dams on day 16 of pregnancy, levels of COX2 and $PGF_{2\alpha}$ significantly rose in $Trp53^{loxP/loxP}Pgr^{Cre/+}$ dams on day 16, 1 day before the onset of preterm birth in these dams. The results suggest that the regulation of uterine LIF and COX2 are different during pregnancy.

p53 has been considered the "guardian of the genome" during pregnancy (57). One major role of the deciduum is to accommodate and support the developing embryo, and the roles of p53 in developing tissues are different from its roles in normal adult tissues or in cancerous tissues. Placental trophoblast cells in direct contact with the deciduum differentiate into large polyploid trophoblast giant cells. There is now evidence that downregulation of p53 leads to terminal differentiation of trophoblast cells (58). Decreased *Trp53* expression with terminal differentiation is also observed in developing organs in mouse embryos (31). These and our present observations suggest differential roles of p53 between adult cells and cells during development.

Because PR is expressed in the myometrium (11), it is possible that myometrial deletion of *Trp53* affects the parturition phenotype in $Trp53^{loxP/loxP}Pgr^{Cre/+}$ dams. However, increased COX2 expression was restricted to decidua in $Trp53^{loxP/loxP}Pgr^{Cre/+}$ dams, but was undetectable in the adjacent myometrium on day 16. Thus, COX2-derived $PGF_{2\alpha}$ produced in the decidua is likely to influence myometrial contractions as a paracrine effector. This would then suggest that decidual changes can be transmitted to the myometrium for initiating labor.

One major advantage of using mice with conditional deletion of uterine *Trp53* over that of systemically *Trp53*-deleted mice is circumvention of the effects on *Trp53*-deleted embryos. Hu et al. found the most implantation failures when they crossed $Trp53^{-/-}$ females with $Trp53^{-/-}$ males (6). This is an important issue in light of the observed anomalies in $Trp53^{-/-}$ embryos (8). Our present study found that decidual senescence and restricted growth was reflected in reduced growth of placentas and fetuses in $Trp53^{loxP/loxP}Pgr^{Cre/+}$ dams. This reduced fetoplacental growth appears secondary to restricted decidual growth, as we did not notice any sign of senescence in placentas or fetuses in $Trp53^{loxP/loxP}Pgr^{Cre/+}$ dams. This observation is consistent with the presence of *Trp53* in placentas and embryos developing in $Trp53^{loxP/loxP}Pgr^{Cre/+}$ dams (Supplemental Figure 13). In addition, the ratio of $Trp53^{loxP/loxP}Pgr^{+/+}$ to $Trp53^{loxP/loxP}Pgr^{Cre/+}$ genotype was comparable between live and dead pups born to $Trp53^{loxP/loxP}Pgr^{Cre/+}$ dams (data not shown), which suggests that fetal death in $Trp53^{loxP/loxP}Pgr^{Cre/+}$ dams is independent of embryo genotype.

Our observations of senescence-associated uterine growth restriction and preterm birth with conditional deletion of uterine *Trp53* have uncovered a critical role of p53 in uterine biology and parturition involving the p21/Akt/COX2 pathway (Figure 7). This may then connect the observations that women at age 35 or older are at higher risk of premature birth (1) and that p53 activity diminishes in mice as they age (59).

Although inflammation and bacterial infection is considered a major cause of preterm labor in humans, many other causes remain unknown. Mice are often used to study the role of inflammation in preterm labor. However, mouse models for studying spontane-

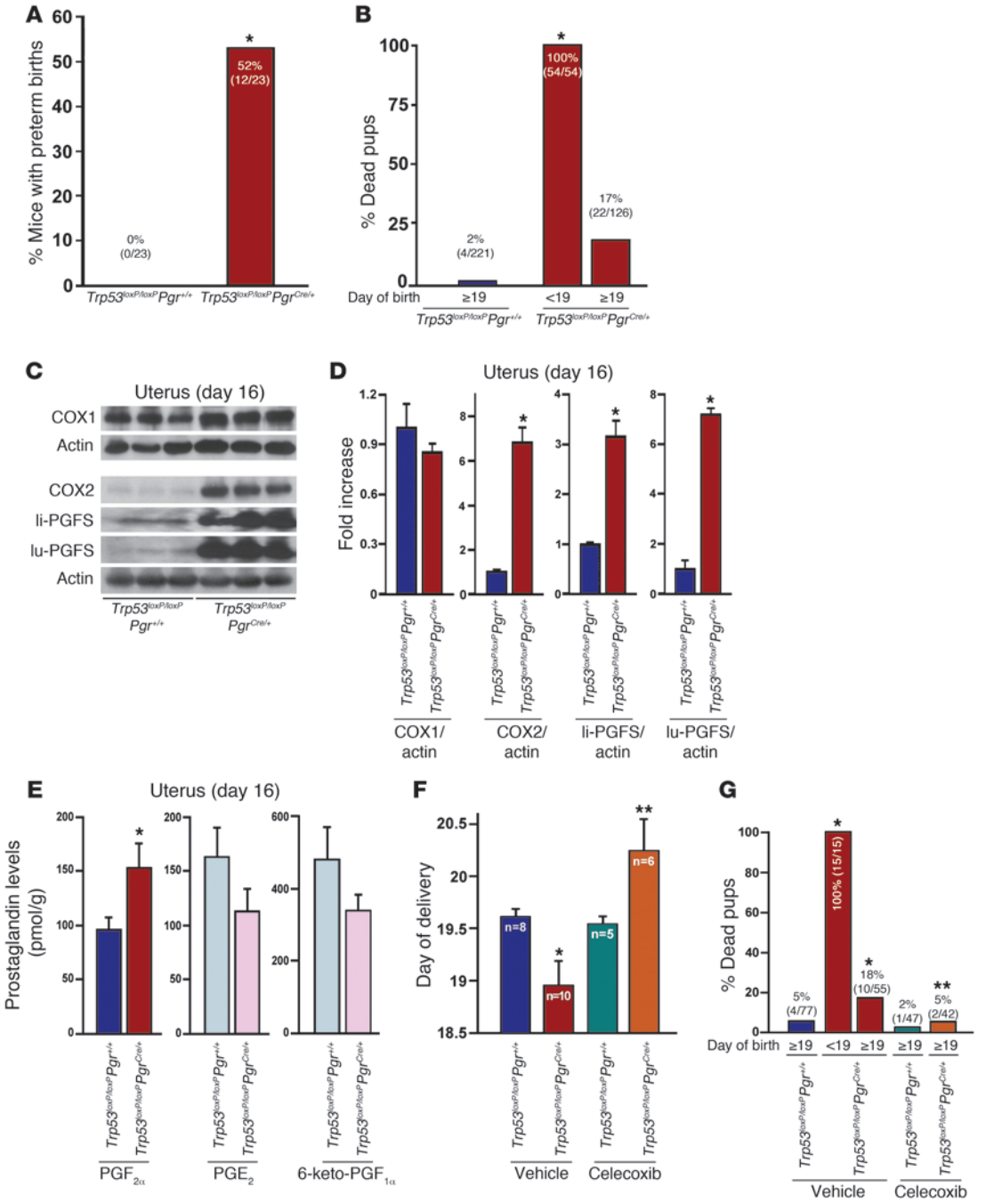

Figure 6

Uterine deletion of *Trp53* promotes preterm birth through COX2/PGFS/$PGF_{2\alpha}$ pathway. (**A**) Preterm birth (deliveries earlier than day 19) occurred in 52% of $Trp53^{loxP/loxP}Pgr^{Cre/+}$ dams (*$P < 0.05$). Numbers in parentheses denote the ratio of dams with preterm birth/total dams. (**B**) All pups born before day 19 were dead around the time of delivery or died immediately after birth (*$P < 0.05$ versus $Trp53^{loxP/loxP}Pgr^{+/+}$). Numbers in parentheses denote the ratio of dead pups/total pups. (**C** and **D**) Levels of COX2 and PGFS were upregulated in day 16 uteri lacking p53. (**C**) Uterine samples from which placentas and fetuses had been removed were used for Western blotting, and (**D**) quantitative analysis of band intensities were all normalized against actin (mean ± SEM of 3 independent samples from different mice; *$P < 0.05$). (**E**) Conditional loss of uterine p53 upregulated $PGF_{2\alpha}$ levels in day 16 uteri. A total of 15 independent samples from 3 different mice were evaluated (mean ± SEM; *$P < 0.05$). (**F** and **G**) Preterm birth and neonatal deaths in $Trp53^{loxP/loxP}Pgr^{Cre/+}$ mice were reversed by oral gavage of celecoxib (10 mg/kg/dose, administered twice) on day 16. In **G**, numbers in parentheses denote the ratio of dead pups/total pups. *$P < 0.05$ versus vehicle-treated $Trp53^{loxP/loxP}Pgr^{+/+}$; **$P < 0.05$ versus vehicle-treated $Trp53^{loxP/loxP}Pgr^{Cre/+}$.

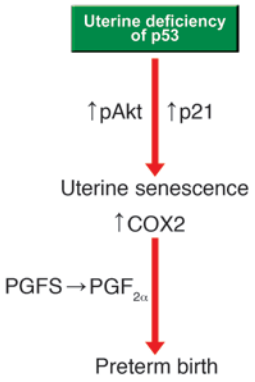

Figure 7
Potential pathways that promote uterine senescence and preterm birth in *Trp53*$^{loxP/loxP}$*Pgr*$^{Cre/+}$ mice.

ous preterm labor are very limited (43), since most mouse models, unlike humans, require P_4 withdrawal for initiating labor. Therefore, we believe *Trp53*$^{loxP/loxP}$*Pgr*$^{Cre/+}$ mice serve as a novel model to study the underlying mechanism of spontaneous preterm labor without P_4 withdrawal, which may be relevant to determining the causes of premature birth in humans.

Methods

Mice. *Trp53*$^{loxP/loxP}$ mice (10), obtained from the Mouse Models of Human Cancers Consortium, *Pgr*$^{Cre/+}$ mice (11), provided by J.B. Lydon and F.J. DeMayo (Baylor College of Medicine, Houston, Texas), and *Lif*$^{+/-}$ mice (16) were used in this study. To generate mice with uterine deletion of *Trp53*, *Trp53*$^{loxP/loxP}$ mice (FVB/129) were crossed with *Pgr*$^{Cre/+}$ mice (C57BL6/129). The breeding scheme for generating mice with uterine deletion of p53 is shown in Supplemental Figure 14. For experiments, littermate *Trp53*$^{loxP/loxP}$*Pgr*$^{+/+}$ and *Trp53*$^{loxP/loxP}$*Pgr*$^{Cre/+}$ mice (F3 generation) and littermate *Trp53*$^{loxP/+}$*Pgr*$^{+/+}$ and *Trp53*$^{loxP/+}$*Pgr*$^{Cre/+}$ mice (F1 generation) on the mixed background were used. CD1 *Trp53*$^{loxP/loxP}$*Pgr*$^{Cre/+}$ females were generated by backcrossing *Trp53*$^{loxP/+}$*Pgr*$^{Cre/+}$ males on a mixed background with CD1 WT females for 10 generations. For the irradiation study, *Trp53*$^{loxP/loxP}$*Pgr*$^{+/+}$ and *Trp53*$^{loxP/loxP}$*Pgr*$^{Cre/+}$ dams were exposed to 9.5 Gy whole-body γ irradiation. RT-PCR, Northern hybridization, Western blotting, and immunostaining of *Trp53* mRNA and p53 protein in uteri of *Trp53*$^{loxP/loxP}$*Pgr*$^{Cre/+}$ mice showed efficient deletion of *Trp53*. All mice used in this investigation were housed in the Cincinnati Children's Hospital Medical Center Animal Care Facility according to National Institutes of Health and institutional guidelines for the use of laboratory animals. All protocols of the present study were reviewed and approved by Cincinnati Children's Hospital Research Foundation Institutional Animal Care and Use Committee.

Analysis of ovulation, fertilization, implantation, and blastocyst transfer. Mice were examined for ovulation, fertilization, and implantation as described previously (14, 36). *Trp53*$^{loxP/loxP}$*Pgr*$^{+/+}$ and *Trp53*$^{loxP/loxP}$*Pgr*$^{Cre/+}$ females were mated with *Trp53*$^{loxP/loxP}$*Pgr*$^{+/+}$ fertile males to induce pregnancy. The day the vaginal plug was formed was considered day 1 of pregnancy. To examine ovulation and fertilization, mice were sacrificed on day 2 of pregnancy, oviducts were flushed with Whitten's medium to recover ovulated eggs, and fertilization was assessed by the number of 2-cell embryos recovered. To examine preimplantation embryo development and oviductal embryo transfer, mice were sacrificed on day 4 of pregnancy and uteri were flushed with Whitten's medium to recover blastocysts. To examine the attachment reaction and implantation, pregnant dams were sacrificed on day 4, 2200 h, and day 5, 0900 h, respectively. Implantation sites were visualized by intravenous injection of a Chicago blue dye solution, and the number of implantation sites — demarcated by distinct blue bands — was recorded. For blastocyst transfer, pseudopregnant recipients were generated by mating females with vasectomized males. Day 4 *Trp53*$^{loxP/loxP}$*Pgr*$^{+/+}$ blastocysts were transferred into day 4 uteri of *Trp53*$^{loxP/loxP}$*Pgr*$^{+/+}$ or *Trp53*$^{loxP/loxP}$*Pgr*$^{Cre/+}$ pseudopregnant recipients, and implantation sites were examined 96 h later (day 8).

Analysis of parturition. Parturition events were monitored from day 17 through day 21 by observing mice daily, morning, noon, and evening. Preterm birth was defined as birth occurring earlier than day 19 of pregnancy. Dystocia was defined as difficult delivery lasting more than 12 hours. The selective COX2 inhibitor celecoxib was suspended in 0.5% (wt/vol) methylcellulose and 0.1% (vol/vol) polysorbate 80 dissolved in water by constant stirring and was given by oral gavage twice on day 16 of pregnancy (10 mg/kg/dose). This dose of celecoxib is known to selectively inhibit COX2 (60). The control group received vehicle alone.

Estrogen treatment. To determine the effects of uterine p53 deficiency on estrogen-induced uterine *Lif* expression, *Trp53*$^{loxP/loxP}$*Pgr*$^{+/+}$ and *Trp53*$^{loxP/loxP}$*Pgr*$^{Cre/+}$ females were ovariectomized and rested for 2 weeks. They were then given a single subcutaneous injection of E_2 (100 ng in 0.1 ml oil per mouse; ref. 14). The control group of mice received only the vehicle (0.1 ml oil). Mice were killed after 24 hours, and uteri were collected for Northern hybridization.

Preparation of decidual cells. Decidual tissues were isolated from day 8 pregnant mice after dissecting out the embryos. Isolated decidual tissues were passed through various gauges of needles to prepare single-cell suspensions for flow cytometry analysis.

In situ hybridization. Paraformaldehyde-fixed frozen sections were hybridized with ^{35}S-labeled cRNA probes as described previously (13). To compare mRNA localization between *Trp53*$^{loxP/loxP}$*Pgr*$^{+/+}$ and *Trp53*$^{loxP/loxP}$*Pgr*$^{Cre/+}$ tissues, sections of tissues from both genotypes were placed onto the same slide and processed for hybridization. Mouse-specific cRNA probes for *Ptgs2*, *Lif*, *Hoxa10*, and *Bmp2* were used for hybridization.

Northern hybridization. Total RNA (6 μg) was denatured, separated by formaldehyde-agarose gel electrophoresis, and transferred onto nylon membranes. Cross-linked blots were prehybridized, hybridized, and washed as described previously (13). ^{32}P-labeled cRNA probes for mouse *Trp53*, *Lif*, *Hoxa10*, *Bmp2*, *Ptges1*, *Ptgis*, *Hpgd*, and *Rpl7* were used for hybridization. The hybrids were detected by autoradiography. *Rpl7* served as a housekeeping gene. The same blots were used for quantitative analyses of each mRNA.

Western blotting. Protein extraction and Western blotting were performed as described previously (12). Antibodies to p53 (Santa Cruz Biotechnology), actin (Santa Cruz Biotechnology), pAkt (Ser473; Cell Signaling), total Akt (Cell Signaling), p110α (Cell Signaling), p21 (Santa Cruz Biotechnology), 20α-HSD (gift from G. Gibori, University of Illinois at Chicago), COX1 (gift from D. DeWitt, Michigan State University, East Lansing), COX2 (Cayman), and liver- and lung-type PGFS (gifts from K. Watanabe, University of East Asia, Shimonoseki, Japan) were used. The same blots were used for quantitative analyses of each protein. Bands were visualized by using an ECL kit (GE Healthcare). Actin served as a loading control.

Immunohistochemistry. Immunostaining of p53, PR, COX2, Ki67, pAkt, cytokeratin, and CD31 was performed in formalin-fixed, paraffin-embedded sections using specific antibodies to p53 (Lab Vision Cooperation), PR (Invitrogen), COX2 (generated in our laboratory), Ki67 (Lab Vision Cooperation), pAkt (Ser473; Cell Signaling), cytokeratin-8 (Developmental Studies Hybridoma Bank), and CD31 (Santa Cruz Biotechnology), as described previously (12). To compare intensity of immunostaining between *Trp53*$^{loxP/loxP}$*Pgr*$^{+/+}$ and *Trp53*$^{loxP/loxP}$*Pgr*$^{Cre/+}$ tissues, tissue sections from both genotypes on each day of pregnancy were processed onto the same slide.

Flow cytometry. Staining of cells for FACS analysis was performed as previously described (29). Cycle TEST PLUS DNA Reagent Kit (BD) was used for DNA ploidy analysis.

SA–β-gal staining. Staining of SA–β-gal activity was performed as described previously (35). To compare the intensity of SA–β-gal staining between $Trp53^{loxP/loxP}Pgr^{+/+}$ and $Trp53^{loxP/loxP}Pgr^{Cre/+}$ tissues, sections of tissues from both genotypes were processed on the same slide. In brief, frozen sections were fixed in 0.5% glutaraldehyde in PBS and stained for 6 hours in PBS (pH 5.5) containing 1 mM $MgCl_2$, 1 mg/ml X-gal, and 5 mM each of potassium ferricyanide and potassium ferrocyanide. Sections were counterstained with eosin.

RT-PCR. RT-PCR was performed as previously described (12). The housekeeping gene *Actb* (which encodes β-actin) was used as an internal control.

Measurement of E_2 and P_4 levels. Mouse blood samples were collected on days 4, 5, 6, 8, 12, and 16 of pregnancy. Serum levels of E_2 and P_4 were measured by EIA kits (Cayman).

Measurement of PG profiles. Implantation sites from which fetuses and placentas had been removed were collected on day 16 of pregnancy. Methanolic extracts of tissues were partially purified by passing through solid phase cartridges, and PGs were quantified by liquid chromatography–tandem mass spectrometry as previously described (61).

Masson trichrome staining. Paraffin-embedded sections were stained with Masson trichrome. Collagen fibrils show blue staining.

Statistics. Statistical analyses were performed using 2-tailed Student's *t* test and Fisher exact probability test as appropriate. *P* values less than 0.05 were considered statistically significant.

Acknowledgments

We thank Erin L. Adams for editing the manuscript. We are grateful to John B. Lydon and Francesco J. DeMayo for providing us with the original breeding pair of *PR-Cre* mice and to Geula Gibori, David DeWitt, and Kikuko Watanabe for providing us with specific antibodies. Flow cytometry analyses were performed in the Flow Cytometry Core at Cincinnati Children's Hospital Medical Center supported by an NIH Center grant (AR47363). This study was supported in part by NIH grants (HD12304, DA006668 and DA01822). Y. Hirota is supported by the Japan Society for the Promotion of Science Postdoctoral Fellowships for Research Abroad.

Received for publication July 1, 2009, and accepted in revised form December 9, 2009.

Address correspondence to: Sudhansu K. Dey, Cincinnati Children's Research Foundation, Division of Reproductive Sciences, MLC 7045, 3333 Burnet Avenue, Cincinnati, OH 45229-3039. Phone: 513.803.1158; Fax: 513.803.1160; E-mail: sk.dey@cchmc.org.

1. Goldenberg RL, Culhane JF, Iams JD, Romero R. Epidemiology and causes of preterm birth. *Lancet*. 2008;371(9606):75–84.
2. Saigal S, Doyle LW. An overview of mortality and sequelae of preterm birth from infancy to adulthood. *Lancet*. 2008;371(9608):261–269.
3. Behrman RE, Butler AS, eds. *Preterm Birth*. Washington, DC: The National Academies Press; 2007.
4. Wang H, Dey SK. Roadmap to embryo implantation: clues from mouse models. *Nat Rev Genet*. 2006; 7(3):185–199.
5. Vogelstein B, Lane D, Levine AJ. Surfing the p53 network. *Nature*. 2000;408(6810):307–310.
6. Hu W, Feng Z, Teresky AK, Levine AJ. p53 regulates maternal reproduction through LIF. *Nature*. 2007;450(7170):721–724.
7. Donehower LA, et al. Mice deficient for p53 are developmentally normal but susceptible to spontaneous tumours. *Nature*. 1992;356(6366):215–221.
8. Sah VP, Attardi LD, Mulligan GJ, Williams BO, Bronson RT, Jacks T. A subset of p53-deficient embryos exhibit exencephaly. *Nat Genet*. 1995; 10(2):175–180.
9. Schwartz D, Goldfinger N, Kam Z, Rotter V. p53 controls low DNA damage-dependent premeiotic checkpoint and facilitates DNA repair during spermatogenesis. *Cell Growth Differ*. 1999;10(10):665–675.
10. Jonkers J, Meuwissen R, van der Gulden H, Peterse H, van der Valk M, Berns A. Synergistic tumor suppressor activity of BRCA2 and p53 in a conditional mouse model for breast cancer. *Nat Genet*. 2001; 29(4):418–425.
11. Soyal SM, et al. Cre-mediated recombination in cell lineages that express the progesterone receptor. *Genesis*. 2005;41(2):58–66.
12. Daikoku T, et al. Conditional loss of uterine Pten unfailingly and rapidly induces endometrial cancer in mice. *Cancer Res*. 2008;68(14):5619–5627.
13. Das SK, et al. Heparin-binding EGF-like growth factor gene is induced in the mouse uterus temporally by the blastocyst solely at the site of its apposition: a possible ligand for interaction with blastocyst EGF-receptor in implantation. *Development*. 1994;120(5):1071–1083.
14. Lim H, et al. Multiple female reproductive failures in cyclooxygenase 2-deficient mice. *Cell*. 1997; 91(2):197–208.
15. Stewart CL, et al. Blastocyst implantation depends on maternal expression of leukaemia inhibitory factor. *Nature*. 1992;359(6390):76–79.
16. Song H, Lim H, Das SK, Paria BC, Dey SK. Dysregulation of EGF family of growth factors and COX-2 in the uterus during the preattachment and attachment reactions of the blastocyst with the luminal epithelium correlates with implantation failure in LIF-deficient mice. *Mol Endocrinol*. 2000; 14(8):1147–1161.
17. Song H, Lim H. Evidence for heterodimeric association of leukemia inhibitory factor (LIF) receptor and gp130 in the mouse uterus for LIF signaling during blastocyst implantation. *Reproduction*. 2006; 131(2):341–349.
18. Yue L, et al. Cyclin G1 and cyclin G2 are expressed in the periimplantation mouse uterus in a cell-specific and progesterone-dependent manner: evidence for aberrant regulation with Hoxa-10 deficiency. *Endocrinology*. 2005;146(5):2424–2433.
19. Cooke PS, Fujii DK, Cunha GR. Vaginal and uterine stroma maintain their inductive properties following primary culture. *In Vitro Cell Dev Biol*. 1987; 23(3):159–166.
20. Lim H, Ma L, Ma WG, Maas RL, Dey SK. Hoxa-10 regulates uterine stromal cell responsiveness to progesterone during implantation and decidualization in the mouse. *Mol Endocrinol*. 1999;13(6):1005–1017.
21. Paria BC, et al. Cellular and molecular responses of the uterus to embryo implantation can be elicited by locally applied growth factors. *Proc Natl Acad Sci U S A*. 2001;98(3):1047–1052.
22. Lee KY, et al. Bmp2 is critical for the murine uterine decidual response. *Mol Cell Biol*. 2007; 27(15):5468–5478.
23. Pohnke Y, et al. Wild-type p53 protein is up-regulated upon cyclic adenosine monophosphate-induced differentiation of human endometrial stromal cells. *J Clin Endocrinol Metab*. 2004;89(10):5233–5244.
24. Yoshino O, et al. Akt as a possible intracellular mediator for decidualization in human endometrial stromal cells. *Mol Hum Reprod*. 2003;9(5):265–269.
25. Astanehe A, et al. Mechanisms underlying p53 regulation of PIK3CA transcription in ovarian surface epithelium and in ovarian cancer. *J Cell Sci*. 2008; 121(Pt 5):664–674.
26. Parker SB, et al. p53-independent expression of p21Cip1 in muscle and other terminally differentiating cells. *Science*. 1995;267(5200):1024–1027.
27. Macleod KF, et al. p53-dependent and independent expression of p21 during cell growth, differentiation, and DNA damage. *Genes Dev*. 1995;9(8):935–944.
28. Tan J, Raja S, Davis MK, Tawfik O, Dey SK, Das SK. Evidence for coordinated interaction of cyclin D3 with p21 and cdk6 in directing the development of uterine stromal cell decidualization and polyploidy during implantation. *Mech Dev*. 2002; 111(1–2):99–113.
29. Cross SM, et al. A p53-dependent mouse spindle checkpoint. *Science*. 1995;267(5202):1353–1356.
30. Baccini V, et al. Role of p21(Cip1/Waf1) in cell-cycle exit of endomitotic megakaryocytes. *Blood*. 2001; 98(12):3274–3282.
31. Schmid P, Lorenz A, Hameister H, Montenarh M. Expression of p53 during mouse embryogenesis. *Development*. 1991;113(3):857–865.
32. Campisi J, d'Adda di Fagagna F. Cellular senescence: when bad things happen to good cells. *Nat Rev Mol Cell Biol*. 2007;8(9):729–740.
33. Chen Z, et al. Crucial role of p53-dependent cellular senescence in suppression of Pten-deficient tumorigenesis. *Nature*. 2005;436(7051):725–730.
34. Li Y, Dowbenko D, Lasky LA. AKT/PKB phosphorylation of p21Cip/WAF1 enhances protein stability of p21Cip/WAF1 and promotes cell survival. *J Biol Chem*. 2002;277(13):11352–11361.
35. Krizhanovsky V, et al. Senescence of activated stellate cells limits liver fibrosis. *Cell*. 2008;134(4):657–667.
36. Tranguch S, Wang H, Daikoku T, Xie H, Smith DF, Dey SK. FKBP52 deficiency-conferred uterine progesterone resistance is genetic background and pregnancy stage specific. *J Clin Invest*. 2007; 117(7):1824–1834.
37. Stocco C, Telleria C, Gibori G. The molecular control of corpus luteum formation, function, and regression. *Endocr Rev*. 2007;28(1):117–149.
38. Challis JR, Lye SJ, Gibb W. Prostaglandins and parturition. *Ann N Y Acad Sci*. 1997;828:254–267.
39. Smith WL, Dewitt DL. Prostaglandin endoperoxide H synthases-1 and -2. *Adv Immunol*. 1996;62:167–215.
40. Helliwell RJ, Adams LF, Mitchell MD. Prostaglandin synthases: recent developments and a novel hypothesis. *Prostaglandins Leukot Essent Fatty Acids*. 2004; 70(2):101–113.

41. Gross GA, et al. Opposing actions of prostaglandins and oxytocin determine the onset of murine labor. *Proc Natl Acad Sci U S A.* 1998;95(20):11875–11879.
42. Winchester SK, et al. Coordinate regulation of prostaglandin metabolism for induction of parturition in mice. *Endocrinology.* 2002;143(7):2593–2598.
43. Ratajczak CK, Muglia LJ. Insights into parturition biology from genetically altered mice. *Pediatr Res.* 2008;64(6):581–589.
44. Sugimoto Y, et al. Failure of parturition in mice lacking the prostaglandin F receptor. *Science.* 1997; 277(5326):681–683.
45. Okita RT, Okita JR. Prostaglandin-metabolizing enzymes during pregnancy: characterization of NAD(+)-dependent prostaglandin dehydrogenase, carbonyl reductase, and cytochrome P450-dependent prostaglandin omega-hydroxylase. *Crit Rev Biochem Mol Biol.* 1996;31(2):101–126.
46. Tai HH, Ensor CM, Tong M, Zhou H, Yan F. Prostaglandin catabolizing enzymes. *Prostaglandins Other Lipid Mediat.* August 2002;68–69:483–493.
47. Roizen JD, Asada M, Tong M, Tai HH, Muglia LJ. Preterm birth without progesterone withdrawal in 15-hydroxyprostaglandin dehydrogenase hypomorphic mice. *Mol Endocrinol.* 2008;22(1):105–112.
48. Gimpl G, Fahrenholz F. The oxytocin receptor system: structure, function, and regulation. *Physiol Rev.* 2001;81(2):629–683.
49. Nishimori K, Young LJ, Guo Q, Wang Z, Insel TR, Matzuk MM. Oxytocin is required for nursing but is not essential for parturition or reproductive behavior. *Proc Natl Acad Sci U S A.* 1996;93(21):11699–11704.
50. Takayanagi Y, et al. Pervasive social deficits, but normal parturition, in oxytocin receptor-deficient mice. *Proc Natl Acad Sci U S A.* 2005;102(44):16096–16101.
51. Donehower LA. The p53-deficient mouse: a model for basic and applied cancer studies. *Semin Cancer Biol.* 1996;7(5):269–278.
52. Ma WG, Song H, Das SK, Paria BC, Dey SK. Estrogen is a critical determinant that specifies the duration of the window of uterine receptivity for implantation. *Proc Natl Acad Sci U S A.* 2003; 100(5):2963–2968.
53. Bhatt H, Brunet LJ, Stewart CL. Uterine expression of leukemia inhibitory factor coincides with the onset of blastocyst implantation. *Proc Natl Acad Sci U S A.* 1991;88(24):11408–11412.
54. Chen JR, Cheng JG, Shatzer T, Sewell L, Hernandez L, Stewart CL. Leukemia inhibitory factor can substitute for nidatory estrogen and is essential to inducing a receptive uterus for implantation but is not essential for subsequent embryogenesis. *Endocrinology.* 2000;141(12):4365–4372.
55. Lim H, et al. Cyclo-oxygenase-2-derived prostacyclin mediates embryo implantation in the mouse via PPARdelta. *Genes Dev.* 1999;13(12):1561–1574.
56. Wang H, et al. Stage-specific integration of maternal and embryonic peroxisome proliferator-activated receptor delta signaling is critical to pregnancy success. *J Biol Chem.* 2007;282(52):37770–37782.
57. Brosens JJ, Gellersen B. Death or survival--progesterone-dependent cell fate decisions in the human endometrial stroma. *J Mol Endocrinol.* 2006; 36(3):389–398.
58. Soloveva V, Linzer DI. Differentiation of placental trophoblast giant cells requires downregulation of p53 and Rb. *Placenta.* 2004;25(1):29–36.
59. Feng Z, Hu W, Teresky AK, Hernando E, Cordon-Cardo C, Levine AJ. Declining p53 function in the aging process: a possible mechanism for the increased tumor incidence in older populations. *Proc Natl Acad Sci U S A.* 2007;104(42):16633–16638.
60. Reese J, Paria BC, Brown N, Zhao X, Morrow JD, Dey SK. Coordinated regulation of fetal and maternal prostaglandins directs successful birth and postnatal adaptation in the mouse. *Proc Natl Acad Sci U S A.* 2000;97(17):9759–9764.
61. Huang SM, et al. Overexpressed transient receptor potential vanilloid 3 ion channels in skin keratinocytes modulate pain sensitivity via prostaglandin E2. *J Neurosci.* 2008;28(51):13727–13737.